

Interaction of C and Mn in a $\Sigma 3$ grain boundary of bcc iron

A T Wicaksono and M Militzer

Centre for Metallurgical Process Engineering, The University of British Columbia, Vancouver, Canada, V6T 1Z4

E-mail: matthias.militzer@ubc.ca

Abstract. The interaction of alloying elements with migrating interfaces is a key aspect that determines microstructure evolution during thermo-mechanical processing of metals and alloys. Recent advances in atomic scale resolution characterization techniques and atomistic modelling have dramatically increased the potential to generate new knowledge on interfaces thereby enabling paradigm shifts in microstructure design approaches. Computational materials science now offers exciting opportunities to formulate multi-scale process models that bridge the gap between atomistic and continuum approaches. In particular, the development of advanced high strength steels with novel alloying concepts has motivated atomistic scale simulations to predict the interaction of selected alloying elements with grain boundaries and the austenite-ferrite interface in iron. Most of these simulations have so far been carried out for binary systems with one solute species. The extension of this modelling work to multi-component systems is, however, essential in order to account for potential interactions between different alloying elements in industrial steels. Here, we present *ab initio* simulations for the interaction of C and Mn at a $\Sigma 3$ boundary in bcc iron using density functional theory (DFT). The simulation results confirm the strong co-segregation of C and Mn that has been recently observed in atom probe tomography studies of the austenite-ferrite interface in Fe-Mn-C alloys.

1. Introduction

The development of modern steels such as advanced high strength steels is aided by a better understanding of the role of alloying elements on the kinetics of the austenite-ferrite transformation. The presence of substitutional solutes, e.g. Mn, Nb and Mo, has been shown to dramatically reduce the velocity of the austenite-ferrite interface during phase transformation via a solute drag effect [1–4]. Accurate prediction of the transformation kinetics is challenging because several aspects contribute to the complexity of solute-interface interactions, including the presence of other solute elements in the interface and the difference in their diffusivities. A number of ferrite growth models have been proposed to account for the solute drag effect in ternary Fe-X-C systems, see [5] for a recent survey. These models are frequently based on an assumption in which the solute-interface interaction is solely attributed through a parameter referred to as the binding energy, which captures the affinity of solute X to the interface.

The single binding energy assumption fails to capture the complex interaction among different types of solute elements. For example, recent work that employed atom probe tomography (APT) [6, 7] found that the enrichment level of Mn at the austenite-ferrite interface in the Fe-Mn-C system is twice the bulk Mn content even though the bulk diffusivity and the binding energy of Mn in general grain boundaries of bcc Fe alone are only in the order of 10^{-17}



m^2s^{-1} at 680°C [7] and 5.5 kJ mol^{-1} [8], respectively. On the other hand, no Mn enrichment at the austenite-ferrite interface was reported for the ternary Fe-Mn-N system [6]. This suggests that the high Mn enrichment in the Fe-Mn-C system may be attributed to the presence of carbon at the interface. Such a hypothesis has also been indicated in earlier work [9, 10], although it remains challenging to verify experimentally.

First principle calculations such as density functional theory (DFT) offer a systematic way to verify the interaction between Mn and C in the bulk, at grain boundaries and bcc-fcc interfaces in Fe. The important role of DFT in alloy design has been demonstrated in a number of efforts that employed modelling across different length and time scales, e.g. development of modern steels [11, 12]. Studies that apply DFT as a modelling tool have largely targeted binary systems, e.g. Fe-C [13–19], Fe-Mn [20, 21], Fe-Cr [16, 22], and Fe-N [11, 15], with little attention dedicated to ternary systems. A few examples of DFT calculations for ternary alloys include a study on the Fe-Cr-C system [16] and another on Fe-Nb-X systems (where $X = \text{Mo, Ti, Cr, Mn}$) [23].

This work aims to focus on the Fe-Mn-C system, with the objective of investigating the interaction between Mn and C in the bulk and at the incoherent $\Sigma 3(111)$ grain boundary (GB) of bcc Fe using DFT. The $\Sigma 3(111)$ boundary is chosen since its structure has a relatively short periodicity, thus providing a reasonable limit on the number of boundary sites that Mn and C can occupy. First, the Mn-C interaction in bulk bcc Fe will be explored as a function of the distance between Mn and C atoms to determine the spatial extent of their interaction. Then, the binding energy of individual Mn and C atoms at a number of boundary sites are computed to identify favourable sites for segregation. Finally, the co-segregation energy of Mn and C atoms for these sites is determined and assessed against recent experiments for the Fe-Mn-C system.

2. Simulation methodology

First-principles spin-polarized calculations are performed using DFT as implemented in the Vienna *ab-initio* Simulation Package (VASP) [24, 25] with the projector-augmented-wave (PAW) method [26]. The exchange correlation functional is modelled using the generalized gradient approximation (GGA) with parameterization by Perdew-Burke-Ernzerhof (PBE) [27, 28]. Targets of 10^{-4} eV and $10^{-2} \text{ eV \AA}^{-1}$ are aimed for energy and force convergence, respectively. The plane-wave basis kinetic cut-off energy is set at 500 eV for all calculations.

Two types of supercells are constructed, namely a bulk bcc and a bicrystal supercell. The bulk supercell consists of 128 lattice sites ($4 \times 4 \times 4$ bcc unit cells) with k -points distributed on a Monkhorst-Pack mesh of $5 \times 5 \times 5$ grids. Periodic boundary conditions are applied in all directions. Bulk calculations show that the lattice parameter of bcc Fe, a , is 2.84 \AA and the energy per Fe atom in the bcc crystal, E_{Fe}^0 , is -8.31 eV (-802 kJ mol^{-1}). These results are consistent with previous calculations [14, 16]. Solute Mn and C are introduced in the bulk bcc Fe as follows. For Mn, an Fe atom is replaced with a Mn atom (e.g. site U in figure 1(a)) whose initial spin orientation is of the opposite sign from that of Fe atoms (i.e. antiferromagnetic configuration following [21, 23]). For carbon, one C atom with a zero spin is placed on an octahedral interstitial site in bcc Fe. In a bulk supercell that contains a Mn and a C atom, the C atom is placed at an octahedral site and the distance $d_{\text{Mn-C}}$ from the Mn atom is varied, e.g. site V ($d_{\text{Mn-C}} = \frac{1}{2}a$) and site W ($d_{\text{Mn-C}} = \frac{1}{2}\sqrt{2}a$) in figure 1(a), up to a distance $d_{\text{Mn-C}}$ of $2.5a$.

A bicrystal supercell is constructed from a set of orthogonal axes that form two $\Sigma 3$ incoherent twin boundaries, where the boundary normal is $\langle 111 \rangle$ and the remaining orthogonal axes are $\langle 112 \rangle$ and $\langle 110 \rangle$, see figures 1(b) and (c). The bicrystal dimensions for subsequent calculations are determined from a size-sensitivity analysis involving supercells of varying dimensions. For a given dimension, the grain boundary energy γ is obtained by taking the difference between the energy of a bicrystal and that of a bulk cell containing an equivalent number of Fe atoms, and normalizing it with the total boundary area of $2L_Y L_Z$. The boundary energy varies less than 0.01 eV \AA^{-2} for bicrystals with dimensions larger than

$L_{X,0} = 4\sqrt{3}a$ (19.6 Å), $L_{Y,0} = 2\sqrt{6}a$ (13.9 Å) and $L_{Z,0} = 2\sqrt{2}a$ (8.0 Å). The bicrystal with dimensions $L_{X,0} \times L_{Y,0} \times L_{Z,0}$ is chosen for subsequent calculations. It contains 192 lattice sites and has a boundary energy γ of 0.46 eV Å⁻² (1.58 J m⁻²), which is consistent with previous work [22].

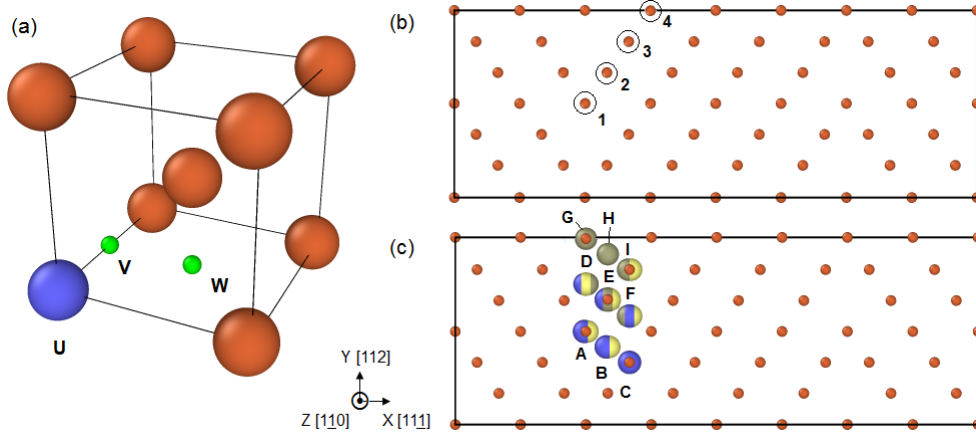


Figure 1. (a) A bcc cell where one atom (U) is highlighted as a substitutional site and two neighbouring octahedral interstitial sites (V and W), (b) A bicrystal that contains two $\Sigma 3(111)$ boundaries with boundary sites labelled as 1, 2, and 3, while site 4 is considered a bulk site, (c) Octahedral sites where blue, yellow and grey sites correspond to sites 1, 2 and 3, respectively. Note, sites G, H and I are equivalent to sites A, B and C, respectively.

In bulk bcc Fe, the interaction between Mn and C atoms separated by a distance $d_{\text{Mn-C}}$ is represented by its solution energy $E_{\text{Mn-C}}^0$, which is defined as

$$E_{\text{Mn-C}}^0(d_{\text{Mn-C}}) = \left(E_{\text{Mn-C},\text{total}}^0 + E_{\text{pure}}^0 \right) - \left(E_{\text{Mn},\text{total}}^0 + E_{\text{C},\text{total}}^0 \right) \quad (1)$$

where the superscript 0 indicates the calculation belonging to a bulk supercell, $E_{\text{Mn-C},\text{total}}^0$ is the total energy of a bulk supercell that contains a Mn and a C atom at a distance $d_{\text{Mn-C}}$ from each other, E_{pure}^0 is the energy of a pure bulk Fe supercell with an equivalent number of Fe atoms, $E_{\text{Mn},\text{total}}^0$ and $E_{\text{C},\text{total}}^0$ are the total energies of a bulk supercell that only contains a Mn or a C atom, respectively. Mn and C atoms favour each other's presence in the bulk Fe if $E_{\text{Mn-C}}^0 < 0$.

In order to assess the co-segregation behaviour of Mn-C, the binding energy of a single solute atom X ($X = \text{Mn}$ or C) in the $\Sigma 3(111)$ boundary, E_X^i , is first computed via [23]

$$E_X^i = \left(E_{X,\text{total}}^i + E_{\text{pure}}^0 \right) - \left(E_{X,\text{total}}^0 + E_{\text{pure}}^{gb} \right) \quad (2)$$

where the superscript i indicates the boundary site i , $E_{X,\text{total}}^i$ is the total energy of a bicrystal that contains a solute X at a boundary site i and E_{pure}^{gb} is the total energy of a bicrystal with only Fe atoms. A negative value of E_X^i indicates that site i is an attractive site for solute X .

The $\Sigma 3(111)$ boundary provides three unique lattice sites for a substitutional atom to reside near the boundary, see figure 1(b). Each substitutional site is associated with six different octahedral sites, consisting of two and four octahedral sites that are $\frac{1}{2}a$ and $\frac{1}{2}a\sqrt{2}$ away from a given boundary site, respectively, as shown in figure 1(c). Octahedral sites further than $\frac{1}{2}a\sqrt{2}$ from a given substitutional site are not considered here. Table 1 summarizes the positions of substitutional and interstitial boundary sites.

Table 1. Positions of substitutional and octahedral sites in the $\Sigma 3(111)$ boundary relative to the coordinate of substitutional site 1 (see figures 1(b) and (c)).

Substitutional (S) or octa- hedral (O) site	Site label	Positions relative to site 1			Distance* [in units of a] to site		
		X	Y	Z	1	2	3
		(in units of a)					
S	1	0	0	0	0	1	1
S	2	$\frac{1}{6}\sqrt{3}$	$\frac{1}{6}\sqrt{6}$	$\frac{1}{2}\sqrt{2}$	1	0	1
S	3	$\frac{1}{3}\sqrt{3}$	$\frac{1}{3}\sqrt{6}$	0	1	1	0
O	A	0	0	$\frac{1}{2}\sqrt{2}$	$\frac{1}{2}\sqrt{2}$	$\frac{1}{2}$	$\frac{1}{2}\sqrt{2}$
O	B	$\frac{1}{6}\sqrt{3}$	$-\frac{1}{12}\sqrt{6}$	$\frac{1}{4}\sqrt{2}$	$\frac{1}{2}$	$\frac{1}{2}\sqrt{2}$	$\frac{1}{2}$
O	C	$\frac{1}{3}\sqrt{3}$	$\frac{1}{12}\sqrt{6}$	$\frac{1}{4}\sqrt{2}$	$\frac{1}{2}\sqrt{2}$	$\frac{1}{2}\sqrt{2}$	$\frac{1}{2}\sqrt{2}$
O	D	0	$\frac{1}{4}\sqrt{6}$	$\frac{1}{4}\sqrt{2}$	$\frac{1}{2}\sqrt{2}$	$\frac{1}{2}$	$\frac{1}{2}\sqrt{2}$
O	E	$\frac{1}{6}\sqrt{3}$	$\frac{1}{6}\sqrt{6}$	0	$\frac{1}{2}$	$\frac{1}{2}\sqrt{2}$	$\frac{1}{2}$
O	F	$\frac{1}{3}\sqrt{3}$	$\frac{1}{6}\sqrt{6}$	0	$\frac{1}{2}\sqrt{2}$	$\frac{1}{2}\sqrt{2}$	$\frac{1}{2}\sqrt{2}$

* the nearest distance between a site i (or its symmetrically equivalent site) and a substitutional site

The segregation energy of a Mn-C pair in the $\Sigma 3(111)$ boundary, $E_{\text{Mn-C}}^{ij}$, is defined as the energy change as a result of bringing a single Mn and a single C atom from the bulk bcc Fe to a substitutional site i and an octahedral site j at the boundary, respectively, i.e.

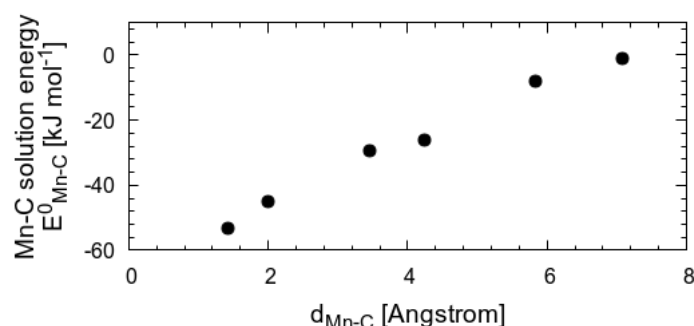
$$E_{\text{Mn-C}}^{ij} = \left(E_{\text{Mn-C},\text{total}}^{ij} - E_{\text{pure}}^{gb} \right) - \left(\left(E_{\text{Mn},\text{total}}^0 - E_{\text{pure}}^0 \right) + \left(E_{\text{C},\text{total}}^0 - E_{\text{pure}}^0 \right) \right) \quad (3)$$

where $E_{\text{Mn-C},\text{total}}^{ij}$ is the total energy of a bicrystal cell that contains an ij pair of Mn-C. The reference states in equation (3) are the binary limits of each solute in bulk bcc Fe, i.e. when Mn and C atoms are sufficiently far apart from each other that they do not interact.

3. Results

3.1. Mn-C interaction in bulk bcc Fe

The bulk solution energy of a Mn-C pair, $E_{\text{Mn-C}}^0$, is plotted in figure 2 as a function of the Mn-C distance. When Mn and C atoms are separated by a distance $d_{\text{Mn-C}}$ of 1.4 Å (0.5 a), the total energy is lowered by 53 kJ mol⁻¹ relative to the case of the binary limits (i.e. when Mn and C are sufficiently far apart from each other that they do not interact). $E_{\text{Mn-C}}^0$ at a distance of 7.1 Å (2.5 a) is -1.1 kJ mol⁻¹, indicating that at this distance the Mn-C pair approaches the interaction limit.

**Figure 2.** Solution energy of Mn-C pair in bcc Fe as a function of the Mn-C distance.

3.2. Grain boundary binding energies of single C and Mn atoms

Figure 3(a) presents the binding energies of a single Mn atom, E_{Mn}^i , on boundary sites 1 to 4 (see figure 1(b)). E_{Mn}^i is the lowest at site 1 (-11 kJ mol^{-1}) and gradually increases to zero at site 4, verifying that site 4 is indeed a bulk site. For comparison, figure 3(a) also presents the binding energy profile for a recently considered $\Sigma 5(310)$ symmetric tilt boundary [23], indicating a number of similarities, including the same order of magnitude of the binding energy. Further, the magnitude of the Mn binding energy at site 1 is about a factor of 2 larger than that obtained from experimental studies on polycrystalline ferrite (-5.5 kJ mol^{-1}) [8].

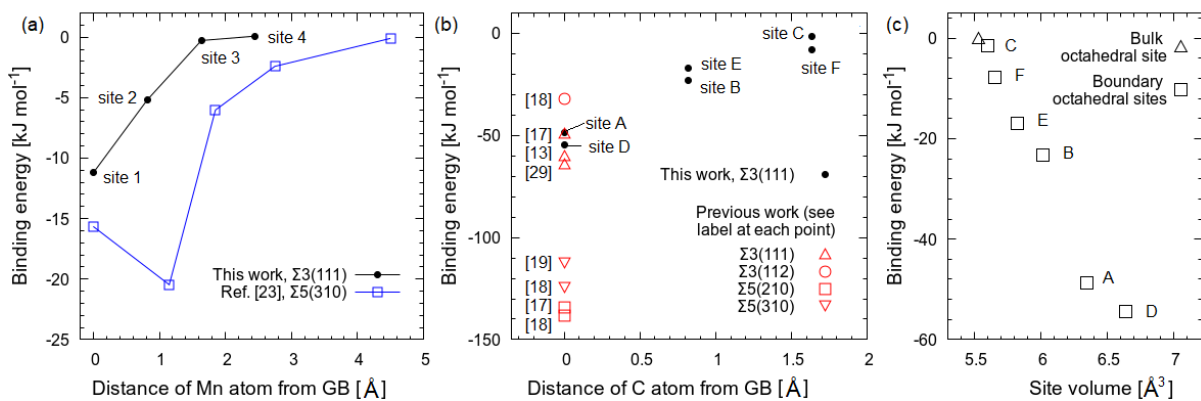


Figure 3. (a) Binding energy profile of a Mn atom from this work and from previous DFT results [23], (b) Binding energy profile of a C atom from this work and previous DFT results [13, 17–19, 29], (c) Relationship between the site volume and the binding energy of a single C atom. See figures 1(b) and (c) for site labels.

Figure 3(b) presents the binding energy profile of a single C atom, E_{C}^i , for octahedral sites A to F (see table 1). DFT results from the literature are also included for comparison. The binding energies of C at zero distance from the $\Sigma 3(111)$ boundary (i.e. -54 and -48 kJ mol^{-1} , see sites A and D in figure 3(b)) are consistent with previous DFT work on the same boundary [13, 17, 29]. The slight discrepancy between our work and Refs. [13, 17, 29] may be attributed to a different cutoff energy for the plane wave basis set and different exchange potential approximations. Finally, the binding energy of C presented here is within the range reported from experiments on general grain boundaries in bcc Fe, i.e. -80 to -30 kJ mol^{-1} [30–33].

The variation of binding energies with different octahedral sites can be rationalized based on the volume of each interstitial site after relaxation, which was obtained using Voronoi tessellation [34]. Figure 3(c) shows the relationship between the site volume and the binding energy of carbon at each site. It is evident that a linear trend emerges, i.e. the magnitude of the binding energy increases with site volume. The correlation between the site volume and the binding energy had also previously been used to rationalize the lower magnitude of binding energies for C in $\Sigma 3$ boundaries as compared to $\Sigma 5$ boundaries [18] (see figure 3(b)) since $\Sigma 3$ boundaries are more compact than $\Sigma 5$ boundaries [17].

3.3. Segregation energy of Mn and C

The segregation energy for each of the 18 ij combinations for the Mn-C pair at the boundary (see table 1) is presented in figures 4(a)-(c). The Mn-C segregation energy ranges from -95 to -51 kJ mol^{-1} and has a profile trend similar to that of the binding energies of single solute atoms shown in figures 3(a) and (b), i.e. $E_{\text{Mn-C}}^{ij}$ is minimum at the boundary and approaches the Mn-C bulk solution energy when the C atom is further away from the boundary. The most preferred

Mn-C configuration at the boundary is pair 1D followed by pairs 3D and 3A. In the latter two cases Mn is a distance of a away from the boundary occupying a site that had negligible attraction in the binary limit (see figure 3a). It is interesting to note that the magnitude of the Mn-C segregation energy for pairs whose carbon atom occupies site D can be up to 40% larger than that of pairs whose carbon atom is on site A (see e.g. pairs 1A and 1D) even though for both pairs all sites are in the boundary plane and the nominal Mn-C distance is the same, i.e. $\frac{1}{2}\sqrt{2}a$ (2 Å). However, the intra-atomic distance of the pair changes after relaxation. For pair 1D, the distance decreases by 10% to 1.8 Å while it increases for pair 1A by 7.5% to 2.15 Å. Further, the interstitial site volume of A is 10% smaller than for site D. The shorter Mn-C distance and larger site volume for pair 1D is consistent with its lower segregation energy as compared to pair 1A. The effective Mn-C distance for other configurations is found to change by less than $\pm 5\%$.

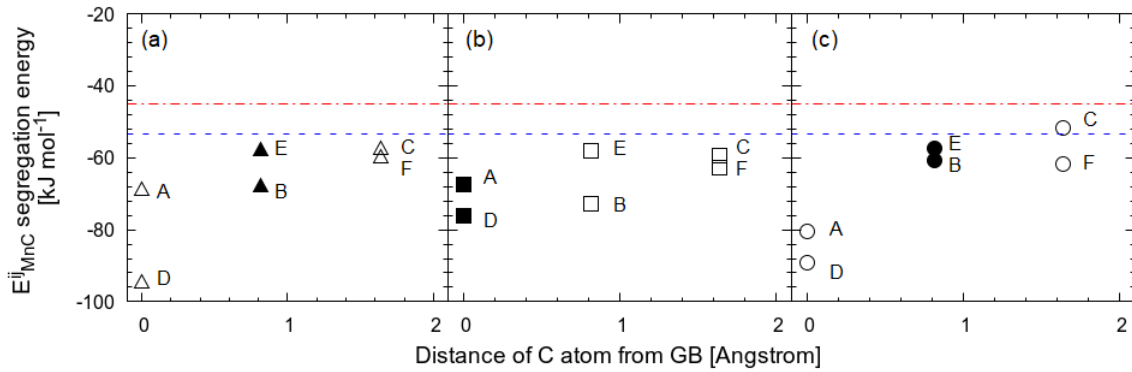


Figure 4. Profile of Mn-C segregation energy for configurations in which the Mn atom is in (a) site 1, (b) site 2, or (c) site 3. The labels (A to F) refer to the site label for the C atom, see table 1. Closed (open) symbols represent Mn-C for $d_{\text{Mn-C}} = \frac{1}{2}a$ ($\frac{1}{2}a\sqrt{2}$). Dashed (dash-dotted) lines indicate $E_{\text{Mn-C}}^0$ when $d_{\text{Mn-C}}$ is $\frac{1}{2}a$ ($\frac{1}{2}a\sqrt{2}$), see figure 2.

4. Discussion

While it is evident from figure 4 that the segregation of Mn and C as a pair to the $\Sigma 3(111)$ boundary is favoured, it is also worth analyzing Mn-C segregation as the sum of its contributions from the binding energy of individual Mn and C atoms and their combined interaction, i.e.

$$E_{\text{Mn-C}}^{ij} = E_{\text{Mn}}^i + E_{\text{C}}^j + \alpha_{ij} \quad (4)$$

where the first two terms on the right hand side correspond to equation(2) and α_{ij} is the Mn-C interaction energy at the boundary. Discussing the Mn-C segregation in terms of α_{ij} is helpful because α_{ij} represents the energy change between the state where Mn and C atoms are at the boundary, within a distance of less than a from each other, and an initial state where they are both at the boundary but sufficiently far apart that they do not interact. As shown in figure 5 the α_{ij} values for all Mn-C configurations range from -60 to -10 kJ mol $^{-1}$. Except for the pairs 2F and 3F, the magnitude of the Mn-C interaction in the boundary is lower than in the bulk (53 kJ mol $^{-1}$). In particular for the preferred configurations of Mn-C segregation (i.e. 1D, 3D, 3A), the interaction term is reduced to about 30 kJ mol $^{-1}$ and has its lowest value for the 1A pair (8 kJ mol $^{-1}$).

The interaction energy α_{ij} can also be used to estimate the co-segregation energy, i.e. the extra binding energy for a given type of solute due to the presence of another type of solute. For example, the co-segregation energy of Mn in site i when there is a C atom in site j is determined

from the sum of the binding energy of Mn in site i , E_{Mn}^i in figure 3(a), and α_{ij} . This suggests that, even though Mn itself has a small binding energy in the $\Sigma 3(111)$ boundary, it gains an extra binding energy from -10 to -60 kJ mol $^{-1}$ if there is a C atom around its vicinity at the boundary. For example, when carbon occupies site D the magnitude of the effective Mn binding energy to site 1 is increased from 11 kJ mol $^{-1}$ to 39 kJ mol $^{-1}$ and for site 3 from 0.5 kJ mol $^{-1}$ to 35 kJ mol $^{-1}$.

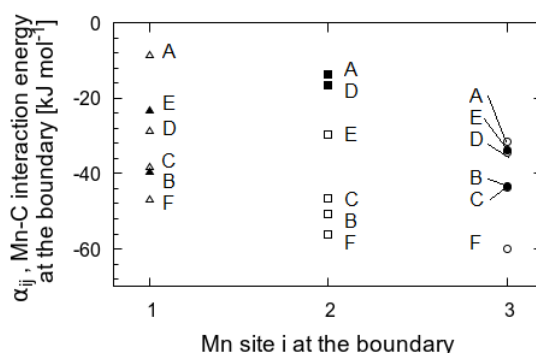


Figure 5. The Mn-C interaction energy at the boundary, α_{ij} , for different Mn-C configurations.

Such an attractive interaction between Mn and C is consistent with recent work using APT [6, 7, 35, 36] which reported high enrichment levels of Mn (a factor of 1.8) at the bcc-fcc interface for the Fe-Mn-C system and no Mn enrichment for the Fe-Mn-N system. The high enrichment level of Mn observed in the Fe-Mn-C system can be rationalized from the fact that C has a relatively high interfacial segregation energy in Fe (about 50 kJ mol $^{-1}$ for the $\Sigma 3(111)$ boundary investigated here) and is a fast diffuser [14]. Both factors contribute to the high segregation level of C at the boundary [18]. The presence of C at the boundary then promotes co-segregation of slower diffusing Mn.

5. Conclusion

We have performed DFT calculations to explore the interaction between Mn and C in bulk bcc Fe and the co-segregation behaviour of Mn and C at a number of boundary sites in a $\Sigma 3(111)$ grain boundary of bcc Fe. Our results demonstrate that Mn and C have an attractive interaction in bulk bcc Fe, with the interaction energy being the strongest (53 kJ mol $^{-1}$) at a Mn-C distance of 1.4 Å, and gradually vanishing at 7.1 Å. Segregation of single C and Mn atoms to a number of $\Sigma 3(111)$ boundary sites show that the maximum magnitude of the binding energies for C and Mn are 54 kJ mol $^{-1}$ and 11 kJ mol $^{-1}$, respectively. These results are within the values reported from previous DFT work and experiments.

That the binding energy of C is higher than the binding energy of Mn implies that C segregation is more favoured than Mn segregation in the Fe-Mn-C system. To explain the high enrichment of Mn experimentally observed in the Fe-Mn-C systems, we examined situations where a Mn and a C atom are located 2 Å from each other in the $\Sigma 3(111)$ boundary. Such Mn-C configurations are found to promote a further energy decrease compared to Mn and C individually segregated at the boundary. The energy change associated with the co-segregation of Mn and C ranges from -60 to -10 kJ mol $^{-1}$, relative to the binding energy of single Mn and C atoms, and depends on the position of the C atom with respect to the boundary and the Mn atom. This finding is consistent with experimental work on Fe-Mn-C alloys which suggest that the high enrichment of Mn at austenite-ferrite interfaces is promoted by carbon segregation.

Acknowledgments

The authors gratefully acknowledge the financial support from the Natural Sciences and Engineering Research Council of Canada and the computing resources provided by WestGrid, a division of Compute Canada.

References

- [1] Zurob H S *et al.* 2008 *Acta Mater* **56** 2203–2211
- [2] Qiu C *et al.* 2013 *Metall. Mater. Trans. A* **44** 3472–3483
- [3] Cahn J W 1962 *Acta Metall.* **10** 789–798
- [4] Hillert M 2004 *Acta Mater.* **52** 5289–5293
- [5] Gouné M *et al.* 2015 *Mater. Sci. Eng. R.* **92** 1–38
- [6] van Landeghem H P *et al.* 2016 *JOM* **68** 1329
- [7] Danoix F *et al.* 2016 *Scr. Mater.* **121** 61–65
- [8] Guttman M 1975 *Surf. Sci.* **53** 213–227
- [9] Mori T 1964 19th committee on reaction in steel making Tech. rep. Department of Metallurgy, Kyoto University
- [10] Jarl M 1978 *Scand. J. Metall.* **7** 93–101
- [11] Wu R, Freeman A J and Olson G B 1994 *Science* **265** 376–380
- [12] Xiong W and Olson G B 2015 *MRS Bulletin* **40** 1035–1044
- [13] Wu R, Freeman A J and Olson G B 1996 *Phys. Rev. B* **53** 7504
- [14] Jiang D E and Carter E A 2004 *Phys. Rev. B.* **67** 214103
- [15] Domain C, Becquart C S and Foct S 2004 *Phys. Rev. B.* **69** 144112
- [16] Sandberg N, Henriksson K O E and Wallenius J 2008 *Phys. Rev. B.* **78** 094110
- [17] Wachowicz E and Kiejna A 2011 *Modell. Simul. Mater. Sci. Eng.* **19** 025001
- [18] Wang J *et al.* 2016 *Acta Mater.* **115** 259–268
- [19] Tahir A, Janisch R and Hartmaier A 2014 *Mater. Sci. Eng. A* **612** 462–467
- [20] Dick A, Hickel T and Neugebauer J 2009 *Steel Research International* **80** 603
- [21] Lintzen S *et al.* 2013 *Journal of Alloys and Compounds* **577** 370–375
- [22] Wachowicz E, Ossowski T and Kiejna A 2010 *Phys. Rev. B.* **81** 094104
- [23] Jin H, Elfimov I and Militzer M 2014 *J. Appl. Phys.* **115** 093506
- [24] Kresse G and Furthmüller J 1996 *Phys. Rev. B* **54** 11169
- [25] Kresse G and Furthmüller J 1996 *Comp. Mater. Sci.* **6** 15–50
- [26] Kresse G and Joubert D 1999 *Phys. Rev. B* **59** 1758
- [27] Perdew J P, Burke K and Ernzerhof M 1996 *Phys. Rev. Lett.* **77** 3865
- [28] Perdew J P, Burke K and Ernzerhof M 1997 *Phys. Rev. Lett.* **78** 1396
- [29] Yamaguchi M 2011 *Metall. Mater. Trans. A* **42** 319–329
- [30] Lejček P and Hofmann S 2016 *J. Phys.: Condens. Matter* **28** 064001
- [31] Papazian J M and Besherb D N 1971 *Met. Trans.* **2** 497–503
- [32] Hänsel B and Grabke H J 1986 *Scr. Metall.* **20** 1641–1644
- [33] Grabke H J 1986 *Steel Research International* **4** 178–185
- [34] Rycroft C H 2009 *Chaos* **19** 041111
- [35] Guo M *et al.* 2015 *Metall. Mater. Trans. A* **46** 2449–2454
- [36] van Landeghem H P *et al.* 2017 *Acta Mater* **124** 536–543